The influence of seasonal land-use-land-cover transformation on thermal characteristics within the city of Pietermaritzburg

Odindi, J.O., S. Nongebeza and N. Siro

School of Agricultural, Earth and Environmental Sciences, University of KwaZulu-Natal, Pietermaritzburg, South Africa, Odindi@ukzn.ac.za

DOI: http://dx.doi.org/10.4314/sajg.v9i2.23

Abstract

Urbanisation has been identified as a major threat to the environment as it increases demand for urban spaces and transforms natural landscapes to impervious surfaces, leading to the Urban Heat Island (UHI) phenomenon. Natural landscapes such as vegetation and water bodies act as thermal sinks that absorb heat while impervious surfaces such as buildings and concrete pavements act as thermal sources that retain and emit heat. The thermal emission results in several negative effects such as temperature inversion, compromised human health, pollution, species loss, high energy consumption and climate change at a local, regional and global scales. Whereas studies on UHI are abound, there is paucity in literature on the influence of seasonal urban Land Use Land Cover (LULC) transformation on urban thermal characteristics. Specifically, the proportional seasonal variability and contribution of individual LULCs to urban heat is often poorly understood. Using the freely available Landsat 8 optical and thermal bands, this study examined the seasonal characteristics of the UHI phenomenon in relation to LULCs in the Pietermaritzburg city, South Africa. Results in this study revealed that UHIs exist in both winter and summer, but with more intensity in summer. The study also established that LULCs varied with seasons. Bare surfaces and dense vegetation had the most thermal influence during winter while dense vegetation and low density buildings had the most thermal influence during summer. These findings provide a better understanding of thermal distribution based on LULC seasonality changes, valuable for sustainable urban planning and climate change mitigation.

Keywords: *Urban Heat Islands, Land Surface Temperature, Seasonal changes, Land cover, Remote sensing.*

1. Introduction

Global population has increased significantly from the mid-20th century, in turn leading to increased urbanisation (Otunga *et al.,* 2014). According to Retief *et al.* (2016), only 2% of the world's population was located in urban areas in the 1800s, currently, approximately 50% (3.4 billion) of the world's population reside in urban areas, a figure projected to reach 70% by 2050 (Aslan and Koc-San, 2016; Ferarall, 2017). Africa has been identified as the fastest urbanizing continent, with a 2.55

million people annual urban population growth (State of South Africa Cities, 2016). In the Sub-Saharan region for instance, urban population was 15% in the mid 20th century, 32% in 1990 and is expected to reach 60% by 2030 (Odindi and Mhangara, 2011).

Whereas urban areas are known to provide multiple opportunities, they are regarded as major drivers to environmental and climatic change. According to Tang & Di (2019), rapid urbanisation and urban land transformation have led to unsustainable growth, urban inequality and environmental deterioration worldwide. Daramola *et al* (2018) and Tang & Di (2019) note that such influx is typically accompanied by conversion of natural sensitive ecosystems to artificial impervious surfaces. This transformation inevitably leads to social and environmental impacts that include loss of natural green spaces and biodiversity, soil erosion, pollution and increase in energy budget (Ayele *et al.,* 2016; Ngie *et al.,* 2016).

Land Use Land Cover (LULC) change arising from urbanization has major implications on local Land Surface Temperatures (LST) and surface moisture regimes, resulting in the formation of Urban Heat Islands (UHI). According to Guo *et al.* (2019), LST plays a vital role in the physics of land surface by regulating atmospheric water and energy exchange. Zhou *et al*. (2014) note that LST influence surface radiative and thermodynamic properties that include surface emissivity, moisture and albedo that alter urban heat flux and moisture, making it vary from the surrounding LULCs or peri-urban landscapes.

Typically, natural landscapes act as thermal sinks, while impervious surfaces thermal sources retain and emit heat (Odindi *et al.,* 2017; Guo *et al.* 2019). Built-up areas such as concrete pavements, tarred roads, and buildings for instance easily take up and trap the sun's energy, which makes urban areas warmer (Gago *et al.,* 2013). Furthermore, urban buildings block wind, which affects the cooling of spaces (Li and Zhao, 2012). Also, the elevated temperature is further intensified by waste from industries, air conditioners, vehicles and other sources (Sailor, 2011). According to Polycarpou (2010), impervious surfaces, when facing the sun, can reach temperatures of about 88℃, whereas vegetation in the same conditions may reach about 18℃. The elevated temperature impact on among others water availability, energy consumption, air quality, human comfort, disease prevalence, mortality and climate (Roth *et al.,* 1989).

The intensity of urban heat varies spatially and temporally within cities, depending on a city's location, landscape mosaic and seasonal patterns (Odindi *et al.,* 2015; Aslan and Koc-San, 2016). UHI occurs in both summer and winter, but are more apparent in winter, especially in the sub-tropic and temperate regions characterised by distinct winter and summer seasons (Aslan and Koc-San, 2016). However, whereas UHI effects and thermal variability on different urban LULCs is widely reported in literature, there is paucity in literature on how LULC contributions vary in winter and summer seasons.

The shortcomings of determining thermal variability within urban landscapes using traditional approaches like total stations, Global Positioning Systems (GPS) and thermal surveys have been widely reported in literature (Adam *et al.,* 2014; Paz-Soldan *et al.,* 2014; Zhou *et al.,* 2014). Hence,

in the recent past, remotely sensed approaches have emerged as an innovative tool to resolve challenges that characterise traditional techniques (Zhou *et al.,* 2014). The growth in the adoption of remote sensing can further be attributed to the high spatial and spectral coverage, decrease in remotely sensed data costs and availability of high quality data (Adam *et al.,* 2014; Mutanga *et al.,* 2016). To date, the Landsat series, Moderate Resolution Imaging Spectroradiometer (MODIS) and Advanced Very High Resolution Radiometer (AVHRR) have particularly been popular in urban LULC/LST studies (Ding and Shi, 2013; Aslan and Koc-San, 2016).

As aforementioned, a large body of literature (e.g. Chow *et al*. 2012, Srivanit *et al.* 2012, Almutairi, 2015) have investigated once-off LULC/LST relationships. However, typically, thermal values vary with seasons. Furthermore, climatic variables like rainfall and temperature vary with season, which in turn influence natural LULCs. This study seeks to augment on existing literature by determining seasonal LULC thermal variability. We hypothesise that urban greenery (e.g. dense vegetation, low vegetation and grasses) and bare areas are characterised by seasonal areal changes, influencing their thermal contribution within an urban landscape. To achieve this objective, we determine the seasonal LULC extents within the city of Pietermaritzburg and then compare their respective seasonal thermal contribution within the city.

2. Materials and Methods

2.1. The study area

The study was conducted in the city of Pietermaritzburg (Figure 1), within uMsunduzi Municipality, KwaZulu-Natal province, South Africa (29º 37′ 40′′S, 30º 23′ 30′′E). Pietermaritzburg is the second largest city in the province, with variable LULC types. It covers approximately 126.15 km². According to the latest Statistics South Africa population count, the city has 618,536 people. The city is located within a bowl-shaped topography with an altitude ranging from 500m to 1130m (Sithole and Odindi, 2015). It is surrounded by mountain ranges that segregate the urban from rural landscapes. The area is characterized by a humid subtropical climate with distinct wet and dry seasons and has an annual precipitation of 900 mm, mainly occurring in mid-summer. Temperatures range from 16-25℃ in winter (May- July), with relatively higher temperatures in summer (November-March) that range between 24 to 37℃. The city's weather is largely influenced by the benign effects of the Indian Oceans equatorial current.

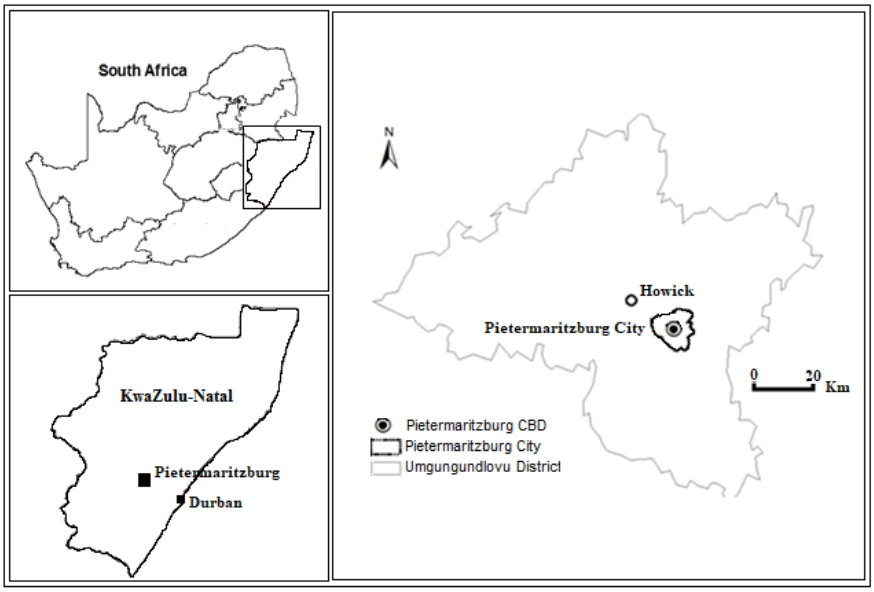

Figure 1: The location of the study area in KwaZulu-Natal province of South Africa.

2.2. Image acquisition and field data collection

The study utilized cloud-free Landsat 8 images (Table 1) with a standard level 1 geometric and radiometric processing. The images were acquired on the 11 February 2017 (summer) and 13 June 2017 (winter) from the United States Geological Survey USGS (www.usgs.gov/earthexplorer). Both images were used to establish the variable LULC types and derivation of LST within the city.

The Landsat 8 OLI/TIRS sensor is characterized by 11 bands with two sensors; the Operational Land Imager (OLI) sensor and Thermal Infrared Sensor. There are nine OLI bands which have a spatial resolution of 30m, except for the panchromatic band 8, which is 15m. The OLI bands used are highly valuable for classifying and mapping the LULC types (Sithole and Odindi, 2015). TIRS, has two thermal bands with a spatial resolution of 100m and were used to extract LST data. In this study, band 3 (Green), 4 (Red) and 5 (Near Infrared) were used for land use land cover mapping while band 10 (Thermal Infrared 1) and 11 (Thermal Infrared 2) were used for thermal mapping.

Table 1: Landsat 8 OLI/TIRS band characteristics

Spectral band	Wavelength (µm)	Resolution (m)
Band 1- Coastal Aerosol	0.43 - 0.45	30
Band 2- Blue	0.45 - 0.51	30
Band 3-Green	0.53 - 0.59	30
Band 4- Red	0.64 - 0.67	30
Band 5- Near Infrared (NIR)	0.85 - 0.88	30
Band 6- Short Wavelength Infrared (SWIR)1	1.57 - 1.65	30
Band 7- Short Wavelength Infrared (SWIR) 2	2.11 - 2.29	30
Band 8- Panchromatic	0.50 - 0.68	15
Band 9- Cirrus	1.36 - 1.38	30
Band 10- Thermal Infrared (TIR)1	10.60 - 11.19	100
Band 11- Thermal Infrared (TIR)2	11.50 - 12.51	100

Google earth pro and the city's aerial photographs for the year 2017 were used to derive the training data. A stratified random sampling approach was adopted to generate a total 250 points from classes listed in table 2 in winter and summer images for classification purposes. This approach was preferred to avoid biasness within the training dataset. The points were separated into 70/30%, where 70% was used for training and 30% for validation

2.3. Data analysis

2.3.1. Image classification

The Maximum Likelihood Classification (MLC) Algorithm was used to classify and discriminate the different LULC types within the city (Adam *et al.,* 2014). The algorithm uses the Bayesian equation to compute the weighted distances or probable likelihood of unknown measurements from known classes (Otukei and Blaschke, 2010). The first step in the classification process was to develop a classification scheme, which consisted of six major LULC classes (i.e. dense and sparse built-up areas, dense and sparse vegetation, water bodies and bare area) within the city (Table 2). The classification was executed using the images and training data in ENVI 5.2.

Table 2: Description of the major LULC classes within with Pietermaritzburg city.

Land-use/Land cover classes	Description
Dense Vegetation	Dense vegetation cover, e.g. Forests
Sparse Vegetation	Grass covered areas with sparse trees and croplands
Dense Built-up	The Central Business District (CBD), industrial areas and dense built-up areas within the city
Sparse Built-up	Moderate to low built-up Residential areas
Water	Water bodies e.g. Rivers, Dams and Ponds)
Bare soil	Bare Areas without cover

2.3.2. Land Surface Temperature (LST) derivation

The Thermal Infrared (TIR) data (Band 10 and 11) were used to derive the LST within the city for both summer and winter. The raster calculator and zonal statistics in ArcGIS were then used to determine the average LST. First, Equation 1 was used to convert the Landsat 8 level 1 Digital Number values into Top Of Atmospheric (TOA) spectral radiance. Equation 2 was then used to covert the spectral radiance to brightness temperatures received by the satellite. Considering that the brightness temperatures were in Kelvins, the third equation was used to convert the brightness temperature from Kelvin to degrees Celsius.

$$L\lambda = MLQcal + AL \quad [1]$$

Where:

Lλ: Spectral radiance (Watts/(m^2 * srad * μm))

ML: Band-specific multiplicative rescaling factor (Radiance_Mult_Band_10)

AL: Band-specific additive rescaling factor (Radiance_Add_Band_10)

Qcal: Quantized and calibrated standard product pixel values (DN) (Ihlen, 2019)

$$BT = \frac{K2}{ln\left(\frac{K1}{L\lambda}+1\right)} \quad [2]$$

Where:

T: At-satellite brightness temperature (Kelvin)

Lλ: Spectral radiance (Watts/(m2 * srad * μm))

K_1: Band specific thermal conversion constant (K1_Constant_Band_10 and 11)

K_2: Band-specific thermal conversion constant (K2_Constant_Band_10 and 11) (Ihlen, 2019)

$$℃ = K - 273.15 \quad [3]$$

Where:

℃: Temperature in Degrees Celsius

K: Temperature in Kelvins

Convert satellite temperature to ground temperature:

$$BT = 1 + W \times \left(\frac{BT}{P}\right) XLn(e) \quad [4]$$

Where:

BT: is at satellite Brightness Temperature calculated in step 2

W: is the wavelength of emitted radiance which is the band 10 radiance

P: is Planks constant (*h*) multiplied by the speed of light (*c*) divide by Boltzmann Constant (1.38×10^{-23} JK^{-1}).

e: is Land Surface Emissivity (LSE) which is defined by NDVI. To get LSE Proportion of vegetation (Pv) was first derived with NDVI using the following formula ($Pv = NDVI - NDVI_{min} \div NDVI_{max} - NDVI_{min})^2$. The outcome was then substituted to the following formula ($e = 0.004 \times Pv + 0.986$) to get LSE. (Ihlen, 2019).

2.4. Surface thermal contribution in the two seasons

The seasonal thermal contribution of the investigated LULC was determined by calculating the differences in LST averages between the cover type and the entire city. The Hawths random point generator was used to extract 500 points within each LULC and respective thermal values. A LULC's thermal contribution to the city was established by multiplying the proportion of the LULC by the difference in the metros average temperature following Chen et al. (2006) Contribution Index (CI) expressed as:

$$CI = Dt \times S \quad [5]$$

Where

CI: is the proportional LST contribution to the entire city,

D_t: is the average LST difference between the cover type and the entire city and S is the proportional area.

2.5. Accuracy Assessment

Using the testing data in ENVI, confusion matrices were generated, which were then used to assess the output classifications for both summer and winter seasons. A kappa statistics was calculated to determine the level of agreement between the classified and training data. In addition, the overall, producer and user accuracies were computed to determine the magnitude of errors in the classification.

$$K = \frac{PO-PE}{1-PE} \quad [6]$$

Where:

K: Kappa coefficient

PO: Probability of Observed

PE: Probability of Expected

2.6. Relationship between temperature and land cover between seasons

To determine the relationship of different LULCs types with temperature, points were generated as described in section 2.4 above. These points were then used to extract points on the four maps (i.e. summer land cover and temperature, and winter land cover and temperature). The tables were then exported to excel for further analyses.

3. Results

3.1. Relationship between land use land covers and temperature

Six major LULC types (Water, Dense vegetation, Grass and small shrubs, High density buildings, Low density buildings and Bare surfaces) were identified in the study area (Table 3 and Figure 2 a and c). High density buildings were concentrated within the city centre and industrial areas located in the south-western part of the city. The most dominant LULC was Low density buildings (LDB), covering 40.92 and 39,43 km^2 of the city's surface area in winter and summer, respectively. LDBs were distributed in most parts of the study area, except the city centre and north-western parts of the city.

The high and low-density vegetation were prevalent in north-eastern part of the city while Bare surfaces were predominantly in the south and south-eastern parts (Figure 2 a and c). As shown on Table 3, the water class, randomly distributed within the city, was the smallest, covering 0.26 Km^2 in winter and 0.74 Km^2 in summer. The highest LULC variability were recorded on Grass and small shrubs (23.85 to 33.93 Km^2) and Bare surfaces (37.17 to 25.00 Km^2) in winter and summer, respectively. Table 3 shows the areal extents of all land cover types within the city.

Table 3: The percentages of winter and summer land use land covers

Land Cover Classes	**Winter**		**Summer**	
	Area in KM^2	% of total area	Area on Km^2	% of total area
Grass and shrubs	23.85	18,91	33.93	26,90
Bare surfaces	37.17	29,47	25.00	19.82
Dense Vegetation	15.06	11,94	18.10	14,35
Water	0.26	0,21	0.74	0,59
High Density buildings	8.87	7,03	8.93	7,08
Low Density Buildings	40.92	32.44	39.43	31,26

Figure 2 shows that the hottest and coolest areas in both seasons were the city's impervious and natural surfaces, respectively.

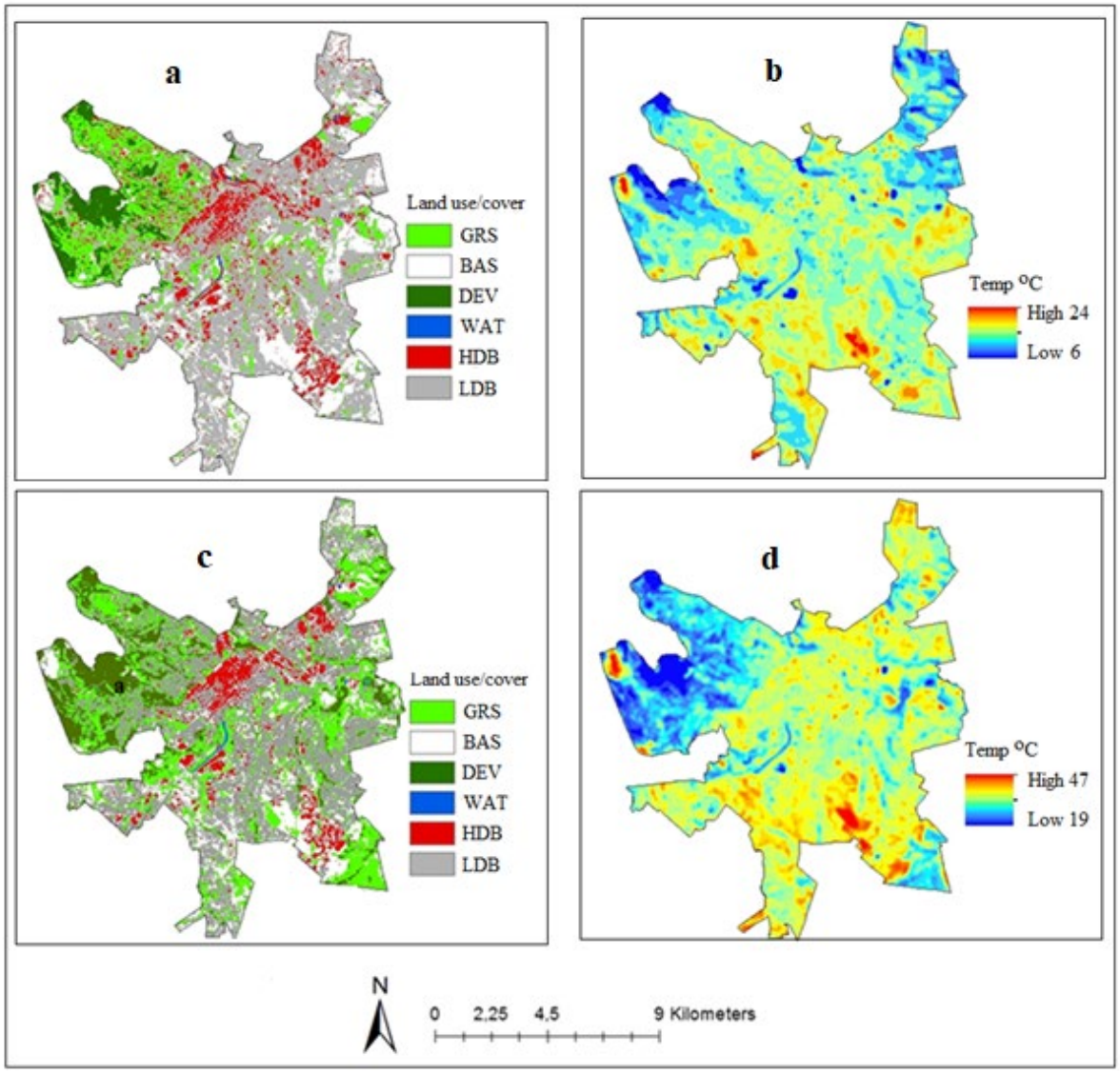

Figure 2: Land cover and temperature distributions – winter (a and b) and summer (c and d), respectively. Low Density Buildings (LDB), High Density Building (HDB), Water (WAT), Dense Vegetation (DEV), Bare Surfaces (BAS), Grass and shrubs (GRS), respectively.

3.2. Land cover accuracy assessment

Tables 4 shows the accuracies achieved in the classification process. The Low-density vegetation class had the lowest classification accuracy while the High-density building class had the highest classification accuracy. Overall, errors of commission had a lower accuracy compared to error of omission. Generally, the overall accuracy requirements will depend on respective landscapes and applications. Whereas Foody (2002) notes that higher accuracies are recommended, Belward *et al.* (1999) notes that above 65% overall accuracy achieved in the global 1- km land-cover data set DISCover would suffice for most contexts.

Table 4: Classification error matrix summary

Land cover	**Accuracy (%)**			
	Winter		**Summer**	
	User	Producer	User	Producer
Water	80	50	100	50
Grass and shrubs	51.2	77.78	48.78	68.75
High-density Vegetation	100	80	100	82.98
Low-density Buildings	51.06	77.78	97.14	84
High-Density buildings	94.74	75	97.4	94.4
Bare Surfaces	77.74	81.4	64	65.79
Overall accuracy	**72.02**		**75.69**	
Kappa	**0.77**		**0.75**	

3.3. The Urban Heat Island (UHI) effect

As expected, average temperature on all land use land cover types were higher in summer than winter. For summer, average temperature were almost 50% higher than winter for the all LULCs. Figure 3 shows the city's seasonal averages.

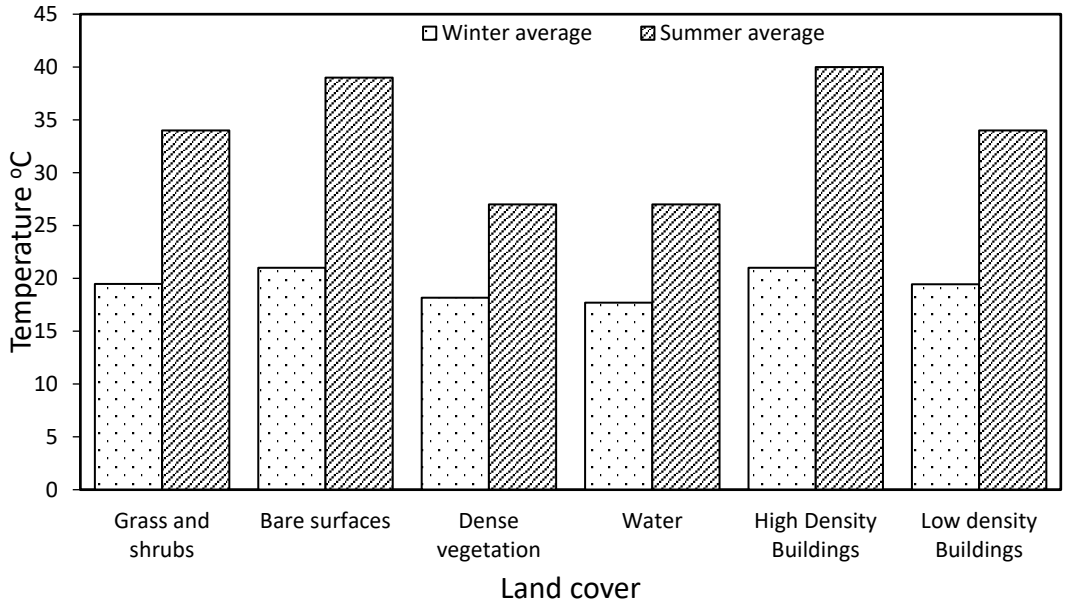

Figure 3: Changes in average temperature across different land cover types between winter and summer. Low Density Buildings (LDB), High Density Building (HDB), Water (WAT), Dense Vegetation (DEV), Bare Surfaces (BAS), Grass and shrubs (GRS).

3.4. Seasonal land use land cover variability

3.4.1. Temperature variability

Figure 4 a and b show seasonal variations in temperature within the LULCs. Low temperatures were recorded in areas with water while higher temperatures were recorded in areas with dense buildings.

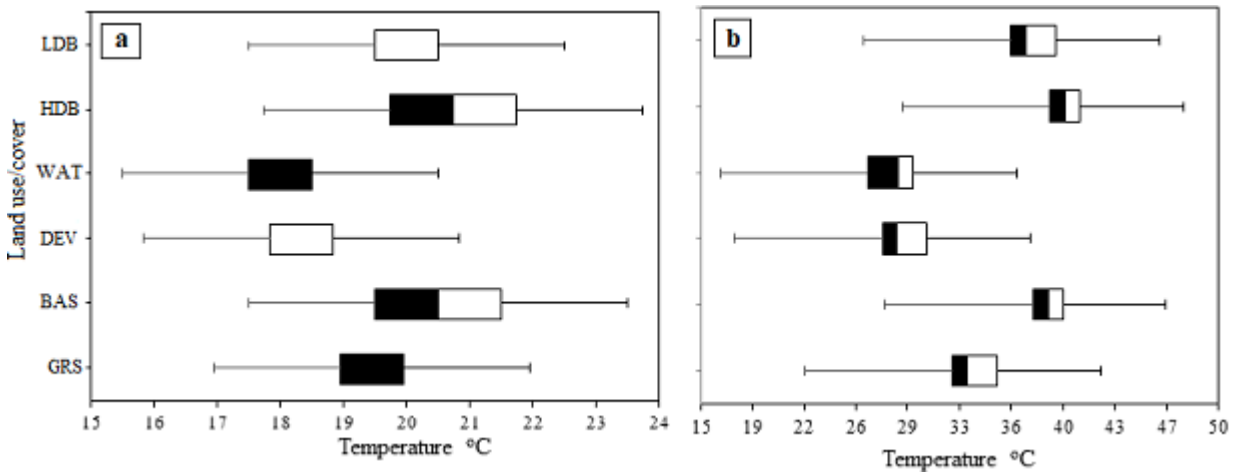

Figure 4: Winter (a) and summer (b) temperature variability across different land cover types. Low Density Buildings (LDB), High Density Building (HDB), Water (WAT), Dense Vegetation (DEV), Bare Surfaces (BAS), Grass and shrubs (GRS).

The contribution of the city's LULCs was based on the LULCs deviation from the season's mean and areal extent. As shown on Figure 5, LULC contributions during winter season were lower than summer. During winter season, positive contributions were shown on grass and shrub and bare surfaces while negative contributions were shown on dense vegetation and water surfaces (Figure 5). During summer, positive contributions were shown on grass and shrub, bare, high density buildings and low density buildings surfaces, while negative contributions were shown on dense vegetation and water surfaces (Figure 5).

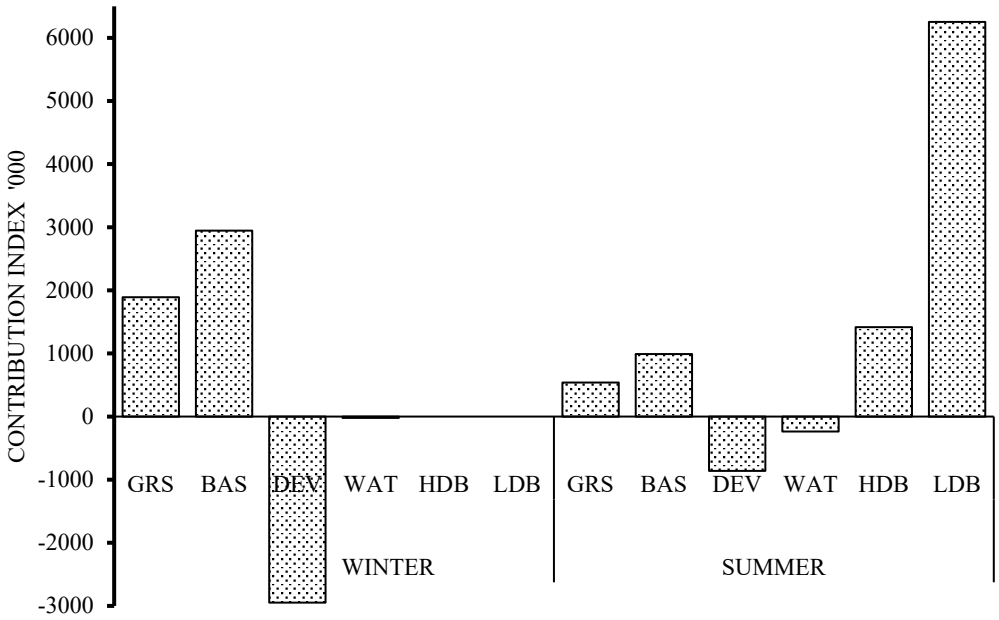

Figure 5: Thermal contribution of major land use/covers during winter and summer. Low Density Buildings (LDB), High Density Building (HDB), Water (WAT), Dense Vegetation (DEV), Bare Surfaces (BAS), Grass and shrubs (GRS).

4. Discussion

Urban areas are largely characterized by impervious surfaces such as roads, buildings and parking spaces. These surfaces act as thermal sources that retain and emit heat, resulting in high temperatures than adjacent non-impervious areas. Cumulatively, this phenomenon is referred to as the UHI. The aim of this study was to determine the implication of seasonal LULC transformation on temperature variation in the Pietermaritzburg city. The freely available Landsat-8 optical and thermal bands were used to determine the city's LULC and LST, respectively.

In consistency with literature e.g. Abutaeb *et al* (2015), Mushore *et al.,* (2017) and Odindi *et al.*, (2017), results in this study showed that the UHI's spatial distribution within the study area is highly dependent on LULC. Furthermore, the findings showed an occurrence of the UHI phenomenon in both seasons, however, intensities and contributions of LULCs were varied. In agreement with existing literature, the study showed that high and low density buildings and bare LULCs had higher thermal values than Water, Dense vegetation and Grass and shrubs LULCs. Studies by Mushore *et al.* (2017) for Harare, Zimbabwe and Odindi *et al.* (2017) for South African coastal metropolitan cities for instance showed that high-density built-up areas were warmer than any other LULCs. Also, in agreement with Abutaleb *et al.* (2015) for the city of Cairo, this study showed that the UHI effect in the city of Pietermaritzburg intensifies in summer than winter, and that the UHI hot and cold spots remain on similar LULCs in the two seasons.

As aforementioned, this study showed that Water and High density vegetation were the city's major cold spots in both seasons. Water, as a cold spot, can be attributed to evapotranspiration and high albedo, however, like most inland global cities, water covers a negligible areal extent (about

0.2%) of the city. Hence, the influence of water as the city's thermal regulator is less significant. The finding on dense vegetation as an urban cold spot is consistent with existing literature (e.g. Abutaleb *et al.,* 2015, Mushore *et al.,* 2017 and Odindi *et al*, 2017). According to Streutker (2002), high density vegetation has a higher albedo compared to built-up areas and bare surface, hence store less heat. Furthermore, the U S Environmrntal Protection Agency (2012) notes that high density vegetation shades the surface from direct solar irradiance which leads to less heat under the canopy. In this study, the difference in thermal assimilation between water and dense vegetation was minimal. This is consistent with Adebowale and Kayode (2015) who noted a minimal thermal difference in areas with high vegetation density and water bodies. The lower thermal values in urban greenery is also consistent with Spronken-Smith *et al*. (2000) who note that natural vegetation within an urban landscape could reduce thermal values by up to 300% in comparison to the adjacent impervious surfaces while United States Environmental Protection Agency (2020) observe that natural urban landscapes, particularly trees, could reduce overlying temperature by 11–25°C. Such reductions have an implication on urban thermal reduction and climate change mitigation. According to Rosenfeld *et al.* (1998), preservation and expansion of natural landscapes within urban areas can reduce thermal values from 32 to 20 °C, in turn reducing ozone values from 240 ppv to 120 ppvb.

The CI results based on LULC's thermal assimilation and emission properties established a high vulnerability to thermal elevation in moderately built up areas during summer (Figure 5). Whereas densely built up areas showed the highest thermal values within the study area, Built-up and Bare surfaces had the highest thermal contribution to the city in the two seasons. This could be attributed to the fact that despite the lower thermal values than the densely built up areas, the low density building's cumulative larger coverage constitute a larger thermal source than any other emitters within the city. According to Rasul *et al*. (2015), bare areas, that include construction sites, often act as a heat source when dry, with similar radiance as densely built LULCs. The bare and moderately built-up areas within urban landscapes lead to greater short-wave absorption due to urban canyon geometry, reduction in net longwave loss and increased heat flux (Oke, 1982). The thermal assimilation and release could also arise from decreased vegetation related evaporation and increased surface roughness, which limits peripheral winds and hinders sensible heat loss (Oke, 1982). This finding suggests that conversion of the landscape to an impervious surface has the greatest thermal influence, with a potential contribution to global warming. Conversely, natural LULCs were the least thermal contributors within the city. This finding is consistent with the impervious surface heat source and natural landscape heat sink that characterize most urban areas. Hence, as suggested by among others Ca *et al*. (1998), Ashie *et al*., (1999), Tong *et al*. (2005) and Yu and Hien (2006), urban sustainability planning should consider urban heat sinks for sustainable urban living. According to Chen *et al*. (2006), consideration of preservation and expansion of natural urban landscapes could off-set the heat generated by built-up areas, valuable for mitigate global warming and climate change.

5. Conclusion

This study aimed to examine the seasonal characteristics of the Urban Heat Island phenomenon using remotely sensed Landsat-8 imagery in concert with GIS in the city of Pietermaritzburg. Generally, the city's LULCs, average temperature and thermal contribution varied in the two seasons. During winter, the study established that low density built up areas and water had the largest and smallest areal spatial extents, respectively during winter. During summer, low density built up areas and water had the largest and smallest areal extents, respectively. Average thermal values varied with LULC types. During winter, densely built up areas and water had the highest and lowest average thermal values, respectively while during summer, densely built up areas and water had the highest and lowest average thermal values, respectively. The contribution of the LULCs to the city's thermal values was mainly dependent on the LULCs spatial extent and type. During winter, the dense vegetation and bare areas were the highest thermal sink and source, respectively, while in summer, the dense vegetation and low-density buildings were the highest thermal sink and source, respectively. This study demonstrates the value of the freely available Landsat 8 imagery in understanding the thermal contribution of urban LULCs, valuable for designing appropriate mitigation measures to address urban challenges like climate change, pollution and urban sustainability. Specifically, the study provides evidence in urban seasonal landscape variability and their thermal implications, a finding that provides for effective adaptability to dealing with urban thermal characteristics. In future, we recommend the adoption of higher spatial resolution thermal datasets to improve the accuracy of urban thermal differences.

6. References

Abutaleb, K., Ngie, A., Darwish, A., Ahmed, M., Arafat, S. and Ahmed, F., 2015, 'Assessment of urban heat island using remotely sensed imagery over Greater Cairo, Egypt', *Advances in Remote Sensing*, vol. *4*(01), pp. 35.

Adebowale, B and Kayode S., 2015, 'Geospatial Assessment of Urban Expansion and Land Surface Temperature in Akure, Nigeria,' 9th International Conference on Urban Climate jointly with 12th Symposium on the Urban Environment Geospatial Assessment of Urban Expansion and Land Surface Temperature, Toulouse, France from July 20-24, 2015.

Adam, E., Mutanga, O., Odindi, J. & Abdel-Rahman, E. M. 2014, 'Land-use/cover classification in a heterogeneous coastal landscape using RapidEye imagery: evaluating the performance of random forest and support vector machines classifiers,' *International Journal of Remote Sensing,* vol. 35(10)**,** pp. 3440-3458.

Almutairi, M.K. 2015, 'Derivation of urban heat island for landsat-8 TIRS Riyadh City (KSA),' *Journal of Geoscience and Environment Protection*, vol. 3, pp. 18–23.

Ashie, Y ., Thanh, V. a& Asaeda, T. 1999, 'Building canopy model for the analysis of urban climate,' *Journal of Wind Engineering and Industrial Aerodynamics*, vol. 81, pp. 237-248.

Aslan, N. & Koc-San, D. 2016, 'Analysis of relationship between urban heat island effect and land use/cover type using landsat 7 etm+ and landsat 8 oli images,' *International Archives of the Photogrammetry, Remote Sensing & Spatial Information Sciences,* vol. 41.

Ayele, G. T., Demessie, S. S., Mengistu, K. T., Tilahun, S. A. & Melesse, A. M. 2016, 'Multitemporal land use/land cover change detection for the Batena Watershed, Rift Valley Lakes Basin, Ethiopia,' *Landscape Dynamics, Soils and Hydrological Processes in Varied Climates.* Springer.

Belward, A. S., Estes, J. E., & Kilne, K. D. 1999, 'The IGBP-DIS global 1- km land-cover data set DISCover: a project overview,' *Photogrammetric Engineering and Remote Sensing*, vol. 65, pp. 1013 – 1020.

Ca, V . T., Asaeda, T. & Abu, E. M. 1998, 'Reductions in air-conditioning energy caused by a nearby park,' *Energy and Buildings*, vol. 29, pp. 83-92.

Chen, X.-L., Zhao, H.-M., Li, P.-X. & Yin, Z.-Y. 2006, 'Remote sensing image-based analysis of the relationship between urban heat island and land use/cover changes,' *Remote Sensing of Environment,* vol. 104(2)**,** pp. 133-146.

Chow, W.T.L., Chuang, W.-C. & Gober, P., 2012, 'Vulnerability to extreme heat in metropolitan Phoenix: spatial, temporal, and demographic dimensions,' *The Professional Geographer*, vol. 64, pp. 286–302.

Daramola, M. T., Eresanya, E. O. & Ishola, K. A. 2018, 'Assessment of the thermal response of variations in land surface around an urban area,' *Modeling Earth Systems and Environment,* vol. 4(2)**,** pp. 535-553.

Ding, H. & Shi, W. 2013, 'Land-use/land-cover change and its influence on surface temperature: a case study in Beijing City,' *International Journal of Remote Sensing,* vol. 34(15)**,** pp. 5503-5517.

Farrell, K. 2017, 'The Rapid Urban Growth Triad: A New Conceptual Framework for Examining the Urban Transition in Developing Countries' , *Sustainability*, vol. 9, pp. 1407-1426

Foody, G. M. 2002, 'Status of land cover classification accuracy assessment', *Remote Sensing of Environment*, vol. 80, pp. 185 – 201.

Gago, E. J., Roldan, J., Pacheco-Torres, R. & Ordóñez, J. 2013, 'The city and urban heat islands: A review of strategies to mitigate adverse effects,' *Renewable and Sustainable Energy Reviews,* vol. 25**,** pp. 749-758.

Guo L, Liu R, Men C, Wang Q, Miao Y. & Zhang Y. 2019, 'Quantifying and simulating landscape composition and pattern impacts on land surface temperature: A decadal study of the rapidly urbanizing city of Beijing, China,' Science of the Total Environment. vol. 654, pp. 430-440.

Ihlen, V. 2019, ' *Landsat 8 (L8) Data Users Handbook*' U.S. Geological Survey, Sioux Falls, South Dakota.

Li, Y. & Zhao, X. 2012, 'An empirical study of the impact of human activity on long-term temperature change in China: A perspective from energy consumption,' *Journal of Geophysical Research: Atmospheres,* vol.117(D17).

Mushore, T.D., Mutanga, O., Odindi, J. and Dube, T., 2017, 'Determining extreme heat vulnerability of Harare Metropolitan City using multispectral remote sensing and socio-economic data,' *Journal of Spatial Science*, pp. 1-19.

Mutanga, O., Dube, T. & Ahmed, F. 2016, 'Progress in remote sensing: vegetation monitoring in South Africa,' *South African Geographical Journal,* vol. 98(3)**,** pp. 461-471.

Ngie, A., Abutaleb, K., Ahmed, F., Taiwo, O., Darwish, A. & Ahmed, M. 2016, 'An estimation of land surface temperatures from landsat ETM+ images for Durban, South Africa,' *Rwanda Journal,* vol. 1(1S).

Odindi, J., Bangamwabo, V. & Mutanga, O. 2015, 'Assessing theValue ofUrbanGreen Spaces inMitigatingMulti-SeasonalUrban Heat usingMODISLand SurfaceTemperature (LST) andLandsat 8 data,' *International Journal of Environmental Research,* vol. 9(1)**,** pp. 9-18.

Odindi, J., Mutanga, O., Abdel-Rahman, E. M., Adam, E. & Bangamwabo, V 2017, 'Determination of urban land-cover types and their implication on thermal characteristics in three South African coastal metropolitans using remotely sensed data,' *South African Geographical Journal,* 99(1)**,** 52-67.

Odindi, J. O. & Mhangara, P. 2011, 'The Transformation of urban built-up areas during South Africa's democartic transition: a case of Port Elizabeth city using Remote Sensing,' *Journal of Sustainable Development in Africa,* vol. 13.

Oke, T. R. 1982, 'The energetic basis of the urban heat island,' *Quarterly Journal of the Royal Meteorological Society*, vol. 108, pp. 1–24.

Otukei, J. R. & Blaschke, T. 2010, 'Land cover change assessment using decision trees, support vector machines and maximum likelihood classification algorithms,' *International Journal of Applied Earth Observation and Geoinformation,* vol. 12**,** pp. S27-S31.

Otunga, C., Odindi, J. & Mutanga, O. 2014, 'Land Use Land Cover Change in the fringe of eThekwini Municipality: Implications for urban green spaces using remote sensing,' *South African Journal of Geomatics,* vol. 3(2)**,** pp. 145-162.

Paz-Soldan, V. A., Reiner Jr, R. C., Morrison, A. C., Stoddard, S. T., Kitron, U., Scott, T. W., Elder, J. P., Halsey, E. S., Kochel, T. J. & Astete, H. 2014, 'Strengths and weaknesses of Global Positioning System (GPS) data-loggers and semi-structured interviews for capturing fine-scale human mobility: findings from Iquitos, Peru,' *PLoS neglected tropical diseases,* vol. 8(6)**,** pp. e2888.

Polycarpou, L. 2010. No more Pavement! The problem of impervious surfaces. https://blogs.ei.columbia.edu/2010/07/13/no-more-pavement-the-problem-of-impervious-surfaces/: (Accessed 12 September 2019).

Retief, F., Bond, A., Pope, J., Morrison-Saunders, A. & King, N. 2016, 'Global megatrends and their implications for environmental assessment practice,' *Environmental Impact Assessment Review,* vol. 61**,** pp. 52-60.

Rosenfeld, A. H., Akbari, H., & Romm, J. J. 1998, 'Cool communities: Strategies for heat island mitigation and smog reduction,' *Energy and Buildings*, vol. 28, pp. 51–62.

Roth, M., Oke, T.R. & Emery, W.J., 1989. Satellite-derived urban heat islands from three coastal cities and the utilization of such data in urban climatology. *International Journal of Remote Sensing*, vol. 10(11), pp. 1699-1720.

Sailor, D. J. 2011, 'A review of methods for estimating anthropogenic heat and moisture emissions in the urban environment,' *International Journal of Climatology,* vol. 31(2)**,** pp. 189-199.

State of South African Cities Report 2016. Johannesburg. http://www.socr.co.za/ [Accessed 29 September 2019].

Streutker, D.R., 2002, 'A remote sensing study of the urban heat island of Houston, Texas,' *International Journal of Remote Sensing*, vol. 23(13), pp. 2595-2608.

Sithole, K., & Odindi, J.O., 2015, 'Determination of Urban Thermal Characteristics on an Urban/Rural Land Cover Gradient Using Remotely Sensed Data,' *South African Journal of Geomatics*, vol. 4(4), pp. 384-396.

Spronken-Smith, R. A., Oke, T. R., & Lowry, W. P. 2000, 'Advection and the surface energy balance across an irrigated urban park,' *International Journal of Climatology*, vol.20, pp. 1033–1047.

Srivanit, M., Hokao, K. & Phonekeo, V. 2012, 'Assessing the impact of urbanization on urban thermal environment : a case study of Bangkok Metropolitan,' *International Journal of Applied Science and Technology*, vol. 2, pp. 243–256.

Tang, J. & Di, L. 2019, 'Past and Future Trajectories of Farmland Loss Due to Rapid

Urbanization Using Landsat Imagery and the Markov-CA Model: A Case Study of Delhi, India,' *Remote Sensing*, vol. 11, pp. 180-197.

Tong, H., Walton, A., Sang, J. & Chan, J. C. (2005), 'Numerical simulation of urban boundary layer over complex terrain of Hong Kong,' *Atmospheric Environment*, vol. 39, pp. 3549-3563

US Environmental Protection Agency, 2020, ' Using Trees and Vegetation to Reduce Heat Islands,',' Retrieved in June 08, 2020, from https://www.epa.gov/heat-islands/using-trees-and-vegetation-reduce-heat-islands

US Environmental Protection Agency, 2012, 'Heat island impacts,' Retrieved in August 30, 2014, from http://www.epa.gov/hiri/impacts/index.htm

Yu, C. & Hien, W. N. (2006), 'Thermal benefits of city parks,' *Energy and Buildings*, vol. 38, pp. 105-120.

Yuan, F. & Bauer, M.E., 2007, 'Comparison of impervious surface area and normalized difference vegetation index as indicators of surface urban heat island effects in Landsat imagery,' *Remote Sensing of Environment*, vol. 106, pp. 375–386.

Zhou, W., Qian, Y., Li, X., Li, W. & Han, L. 2014, 'Relationships between land cover and the surface urban heat island: seasonal variability and effects of spatial and thematic resolution of land cover data on predicting land surface temperatures,' *Landscape Ecology,* vol. 29(1)**,** pp. 153-167.